

Breakdown of the lattice polaron picture in $\text{La}_{0.7}\text{Ca}_{0.3}\text{MnO}_3$ single crystals

S. H. Chun^{1*}, M. B. Salamon¹, Y. Tomioka², and Y. Tokura^{2,3}

¹ *Department of Physics and Materials Research Laboratory, University of Illinois at Urbana-Champaign, Urbana, Illinois 61801-3080, USA*

² *Joint Research Center for Atomic Technology (JRCAT), Tsukuba 305, Japan*

³ *Department of Applied Physics, University of Tokyo, Tokyo 113, Japan*

(October 31, 2018)

Abstract

When heated through the magnetic transition at T_C , $\text{La}_{0.7}\text{Ca}_{0.3}\text{MnO}_3$ changes from a band metal to a polaronic insulator. The Hall constant R_H , through its activated behavior and sign anomaly, provides key evidence for polaronic behavior. We use R_H and the Hall mobility to demonstrate the breakdown of the polaron phase. Above $1.4T_C$, the polaron picture holds in detail, while below, the activation energies of both R_H and the mobility deviate strongly from their polaronic values. These changes reflect the presence of metallic, ferromagnetic fluctuations, in the volume of which the Hall effect develops additional contributions tied to quantal phases.

It is now well established that the insulator-metal transition and accompanying colossal magnetoresistive effect (CMR) in doped LaMnO_3 arise as small lattice polarons, stable at high temperature, give way to band conduction at low temperature¹. The process by which this occurs is, of course, the key to understanding this and many similar materials in which charge, lattice, orbital, and spin degrees of freedom are intimately linked. The breakdown of the band structure is readily identified with the temperature at which a rapid increase in resistance and the onset of strong negative magnetoresistance arises in well-prepared single crystal samples. Less evident is the temperature at which the small-polaron picture ceases to be valid and, indeed, the nature of charge carriers in the transition region between the two. Recently De Teresa et al. detected the presence of small ferromagnetic clusters below $1.8T_C$ ². However, the way they participate in the macroscopic transport properties remains poorly understood. A possible picture, based on resistivity and thermopower data, suggests that the two phases, polaronic insulator and band metal, coexist and that the metallic concentration increases as magnetic order sets in, resulting in a percolation transition³.

A key piece of evidence for the high temperature polaronic phase comes from Hall effect measurements. At high temperature ($> 1.4T_C$) previous results⁴ found the Hall constant to be negative, despite the hole doping of the material, with the Hall constant $R_H = \rho_{xy}(B)/B$ showing activated behavior with characteristic energy $E_H \approx \frac{2}{3}E_\sigma$, where E_σ is the activation energy for ordinary conductivity σ_{xx} . These results are in accord with the theory of adiabatic hopping of small polarons⁵. It is natural, therefore, to seek evidence for the breakdown of the small-polaron phase in the behavior of the Hall resistivity $\rho_{xy}(B)$ as the temperature approaches the simultaneous insulator-metal/ferromagnetic transition. As we will show, the activation energy changes abruptly at $1.4T_C$ from the polaronic value of $\frac{2}{3}E_\sigma$ to a much larger value, $1.7E_\sigma$, clearly marking the breakdown of the lattice polaron picture in a transport property. In fact, the effective activation energy of the conductivity begins to decrease from E_σ at roughly the same temperature, making the discrepancy even greater. Yet more dramatically, the product of the Hall mobility and temperature $\mu_H T = -\sigma_{xx} R_H T$, which should decrease monotonically with decreasing temperature, in fact exhibits a minimum at

this same cross over temperature. We have argued elsewhere that Hall effect near T_C arises from the combined effect of the double exchange mechanism, in which the spin of the charge carrier must follow the local magnetization, and the partial, but nonuniform, magnetic order that arises near the ferromagnetic transition⁶. Well below T_C , where metallic conductivity dominates, the Hall effect resembles that expected for a metallic ferromagnet.

To carry out this study, we have measured the longitudinal and transverse (Hall) resistivity and the magnetization of $\text{La}_{0.7}\text{Ca}_{0.3}\text{MnO}_3$ single crystal samples ($T_C = 216.2$ K), spanning the full temperature range, from metallic ferromagnet to insulating paramagnet. High quality single crystals of $\text{La}_{0.7}\text{Ca}_{0.3}\text{MnO}_3$ were prepared by the floating-zone method. Electron Probe Micro Analysis revealed a slight deficiency of Ca by 0.01, which partially explains the lower transition temperature compared to polycrystalline samples; details of the growth conditions can be found elsewhere⁷. The specimen used in this experiment has a bar shape with dimensions of $3 \times 1 \times 0.24$ mm³. Contact pads for Hall resistivity measurements were made by sputtering ≈ 1500 Å of gold through a mask. Gold wires were then attached using slowly drying silver paints. The contact resistances after annealing were about 1Ω at room temperature. We adopted both a low frequency ac and a dc method for the measurements. The transverse voltage signal was first nulled at zero field at each temperature by a potentiometer and the change in the transverse voltage recorded as H was swept from +7 T to -7 T and back for averaging. Following the transport measurements, the magnetization was measured by a 7 T SQUID magnetometer on the same sample.

The longitudinal resistivity of our crystal is shown as a function of temperature in the inset of Fig. 1 for two different fields. The small resistivity at low temperature ($\rho_{xx}^0 \approx 140 \mu\Omega\text{cm}$ at 10 K) and the sharp insulator-metal transition indicate the high quality of the crystal used in this experiment. We tentatively divide the temperature into three different regions according to the behavior of ρ_{xx} . In region I (metallic region, below 200 K) ρ_{xx} shows metallic behavior; a term proportional to T^2 dominates the temperature dependence and has been ascribed to electron-electron⁸ or one-magnon scattering processes⁹. The magnetoresistance (MR), defined as $[\rho_{xx}(H = 0) - \rho_{xx}(H = 7 \text{ T})] / \rho_{xx}(H = 7 \text{ T})$, is negligible in this

region. In region II (transition region, between 200 K and 300 K) ρ_{xx} increases sharply and shows a maximum at 230 K. The insulator-metal transition temperature T_{IM} , defined by the peak in $d\rho_{xx}/dT$, is 222.5 K. Although this transition is accompanied by paramagnet-to-ferromagnet transition, T_{IM} is a few degrees higher than the Curie temperature $T_C = 216.2$ K, determined by scaling analysis of high field dc magnetization. The application of high magnetic field reduces ρ_{xx} drastically, thus producing CMR. The maximum reduction occurs at 230 K, the resistivity peak temperature, where ρ_{xx} decreases to less than 4% of its zero field value under 7 T (MR = 2600 %).

The high temperature behavior of ρ_{xx} is well described by small polaron hopping theory in region III (polaron region, above 300 K). In the adiabatic regime, the conductivity is given by

$$\sigma_{xx} \equiv \frac{1}{\rho_{xx}} = \sigma_0 \exp(-E_\sigma/k_B T), \quad (1)$$

and $\sigma_0 = g_d e^2 \nu_0 \delta / a k_B T$. Here, ν_0 and a are the attempt frequency and hopping distance, respectively. We take a to be the Mn-Mn spacing, 0.39 nm. The factor g_d is determined by hopping geometry and δ is the carrier concentration per Mn site⁵. The large value of our prefactor $\sigma_0 \approx 4000 \text{ } \Omega^{-1} \text{cm}^{-1}$ at 300 K confirms the applicability of the adiabatic limit. From the fit to the zero-field data, we have $E_\sigma = 106$ meV, a typical value in this system⁴. The characteristic frequency ν_0 is 1.5×10^{13} Hz if we use $g_d = 5$ and $\delta = 0.3$, and is close to optical phonon frequencies of Mn-O-Mn bond bending (1.4×10^{13} Hz) and stretching (1.9×10^{13} Hz)¹⁰. As the temperature is reduced, the data deviate from Eq. (1) and large magnetoresistivity sets in. We concentrate in the remainder of this paper on the breakdown of small-polaron dynamics at the boundary between regions II and III.

The main panel of Fig. 1 shows the field dependence of ρ_{xy} at several temperatures. The general behavior shares the common features found in other crystals^{11,12} and thin films^{13,14}. At low temperatures (region I) the behavior is not dissimilar to a band ferromagnet: ρ_{xy} decreases initially due to the anomalous Hall effect (AHE) and then increases above 1 T due to the ordinary Hall effect (OHE) of hole-doped material. In region II (transition region),

ρ_{xy} is a strongly non-linear function of field. Finally, in region III, ρ_{xy} is again linear in B , but the slope is now negative.

The Hall effect due to the adiabatic hopping of small polarons was first treated by Emin and Holstein⁵. In that model, the Hall effect arises from interference between direct and indirect hops between two sites via neighboring sites. The trajectory around visited sites encloses magnetic flux, and the interference arises from the Aharonov-Bohm phase thereby induced. When that trajectory involves an odd number of sites, the Hall effect is always negative. Indeed, in region III, the low-field limit of the Hall coefficient $R_H \equiv \rho_{xy}/B$ is negative, an effect observed previously by Jaime et al.⁴ on film samples with lower transition temperatures. It was argued in that paper that both the magnitude of σ_0 and the sign of the Hall effect point to direct Mn-Mn hops and, as a result, to three-site hopping trajectories, and to the introduction of the geometrical factor g_d in the expression for σ_0 . Extending the Emin-Holstein model to this geometry leads to the prediction,

$$R_H = -\frac{g_H}{g_d} \left(\frac{F(J/k_B T)}{ne} \right) \exp \left(\frac{E_H}{k_B T} \right), \quad (2)$$

where $E_H = (2E_\sigma + E_s - J)/3$; J is the magnitude of the transfer integral; E_s , the chemical potential of polarons; and F , a dimensionless function of temperature. We set the geometrical factor $g_H = 2/5^4$, and estimate $J - E_s$ from the band width and thermopower to be $\lesssim 20$ meV. As we can see in Fig. 2, $R_H(T)$ agrees well with the small polaron theory in for temperatures above 300 K. The slope gives $E_H = 73 \pm 7$ meV as compared with $(2E_\sigma + E_s - J)/3 \geq 65$ meV. The lower curve in Fig. 2 shows that E_σ is constant over the same temperature range (note the inverted scale). From the prefactor in Eq. (2) we estimate a carrier density $n \simeq 2.3 \sim 3.7 \times 10^{27} \text{ m}^{-3}$ (depending on the magnitude of J), close to the nominal doping level $5.0 \times 10^{27} \text{ m}^{-3}$.

The Hall coefficient $|R_H|$ increases more rapidly below 300 K with an effective activation energy $\simeq 1.7E_\sigma$, while the effective activation energy of the longitudinal conductivity decreases. This deviation from the small polaron theory can be seen even more clearly in the Hall mobility $\mu_H \equiv R_H/\rho_{xx}$ which measures the excess jump rate induced by the applied

field. We expect $\mu_H T$ to decrease monotonically as the temperature is reduced, with an activation energy $E_\mu \sim (E_\sigma - E_s + J)/3 \leq 41$ meV. As shown in the inset of Fig. 2, $\mu_H T$ decreases as the system cools to $T = 300$ K, with activation energy $E_\mu \approx 33$ meV, but then *increases* on further cooling. Note that $E_H + E_\mu = E_\sigma$, as predicted by small-polaron theory. Another advantage of using μ_H comes from the fact that it is almost field-independent above T_C ^{13,15}, so that the crossover behavior around 300 K is not subject to a low field constraint. The simultaneous decrease in the effective activation energy E_σ and increase in field-induced hopping measured by the Hall mobility points to a fundamental change in carrier behavior. Within the double-exchange model, hole motion is enhanced when neighboring core spins are more nearly aligned. This suggests that local magnetic fluctuations, which grow and become slower with decreasing temperature, lead to more rapid carrier motion within the fluctuation volume. As a consequence, the material enters a two-phase regime in which more conducting regions accompany magnetic fluctuations and at the same time open a new channel for Hall mobility arising from the constraint that the hopping carrier follow the local spin texture. In this picture, small-polaron behavior disappears only when spin correlations increase to the point that they dominate lattice effects, with the features observed near $1.4T_C$ marking that boundary.

Below T_C , the sample becomes increasingly metallic, and we can discuss the Hall effect in the terms usually used for ferromagnetic metals¹⁶, namely as a sum of ordinary $[R_0(T)]$ and anomalous $[R_S(T)]$ Hall contributions

$$\rho_{xy}(B, T) = R_0(T) B + \mu_0 R_S(T) M(B, T), \quad (3)$$

At 10 K, we find $R_0 = 2.3 \times 10^{-10} \text{ m}^3/\text{C}$ which, if we assume the free electron model, corresponds to an effective charge carrier density $n_{eff} = 1/eR_0 = 2.7 \times 10^{28} \text{ m}^{-3}$ or 1.6 holes/Mn, much larger than the nominal doping level (0.3 holes/Mn). Large effective carrier densities have been observed commonly in other crystals and thin films^{11–14} and can be explained when details of the Fermi surface are taken into account¹². Because R_0 is constant in region I, we can easily subtract it from the data to obtain R_S . In regions II and III, the separation

between R_0 and R_S is less clear. However, a fit to Eq. 3 in similar materials showed that R_S was more than an order of magnitude larger than R_0 near T_C ¹². Moreover, $\mu_0 M$ is much larger than B at low fields through region II and the initial part of region III. Thus, in those regions, we take the low-field values of $\rho_{xy}/\mu_0 M$ as R_S and superpose a plot of R_S , normalized to its peak value, and the longitudinal resistivity ρ_{xx} , similarly normalized in Fig. 3. The inset shows the data on a linear plot, and it appears that R_S is proportional to ρ_{xx} , and that the anomalous Hall effect is dominated by skew-scattering¹⁷ in region I. However, when plotted on a logarithmic scale in the main panel, it is clear that there are strong deviations, and that the anomalous Hall effect in region I is proportional to ρ_{xx}^2 , which is the signature of side-jump processes¹⁸. While it may appear that R_S is proportional to ρ_{xx} in region II, we will argue elsewhere that this regime is dominated by the effect of a Berry-like (Pancharatnam) phase induced by the Hund's rule constraint that the hopping charge carrier follow the local magnetic texture⁶. The deviation in region III we attribute, of course, to the OHE of polarons.

In conclusion, Hall-effect data on $\text{La}_{0.7}\text{Ca}_{0.3}\text{MnO}_3$ single crystal samples reveal clear evidence for the boundary between a small-lattice-polaron picture, valid at temperatures greater than $1.4T_C$, and more complex behavior signalling the onset of metallic behavior. In a double exchange ferromagnet above its Curie temperature, local ferromagnetic correlations are enabled by carrier hopping. Localization of the carrier reduces those correlations, lowering the magnetic free energy mainly through an increase in spin entropy¹⁹. In the presence of a tendency for lattice-polaron formation, the entropy term tips the free energy balance toward polaron collapse^{20,21}. Once small polarons form, the underlying antiferromagnetic interactions favor local spin arrangements that suppress Pancharatnam-phase contributions to the Hall effect, leaving essentially pure polaronic behavior. Therefore, the deviation of the Hall resistivity from the polaron term Eq. (2) and the associated reduction of the effective activation energy for ordinary conductivity mark the limit of small-polaron behavior. Below that temperature, the system is a composite of a small-polaron background increasingly filled by ferromagnetic fluctuations that are more highly conducting and that have a Hall

resistivity dominated by local spin texture. The insulator-metal transition then proceeds by a thermally-driven percolation transition.

This work was supported in part by DOE DEFG-91ER45439. We acknowledge helpful discussions with Y. Lyanda-Geller and P. Goldbart.

REFERENCES

- * Present address: Department of Physics, The Pennsylvania State University, University Park, PA 16802-6300.
- ¹ A. P. Ramirez, J. Phys.: Condens. Matter **9**, 8171 (1997).
- ² J. M. De Teresa et al., Nature **386**, 256 (1997).
- ³ M. Jaime et al., Phys. Rev. B **60**, 1028 (1999).
- ⁴ M. Jaime et al., Phys. Rev. Lett. **78**, 951 (1997).
- ⁵ D. Emin and T. Holstein, Ann. Phys. (N.Y.) **53**, 439 (1969).
- ⁶ S. H. Chun, M. B. Salamon, Y. Lyanda-Geller, P. M. Goldbart, and P. D. Han, Phys. Rev. Lett. **84**, 757 (2000).
- ⁷ Y. Tomioka, A. Asamitsu, and Y. Tokura, in preparation.
- ⁸ A. Urushibara et al., Phys. Rev. B **51**, 14 103 (1995).
- ⁹ M. Jaime, P. Lin, M. B. Salamon, and P. D. Han, Phys. Rev. B **58**, R5901 (1998).
- ¹⁰ S. Yoon et al., Phys. Rev. B **58**, 2795 (1998).
- ¹¹ A. Asamitsu and Y. Tokura, Phys. Rev. B **58**, 47 (1998).
- ¹² S. H. Chun, M. B. Salamon, and P. D. Han, Phys. Rev. B **59**, 11 155 (1999).
- ¹³ P. Matl et al., Phys. Rev. B **57**, 10 248 (1998).
- ¹⁴ G. Jacob, F. Martin, W. Westerburg, and H. Adrian, Phys. Rev. B **57**, 10 252 (1998).
- ¹⁵ S. H. Chun, M. B. Salamon, and P. D. Han, J. Appl. Phys. **85**, 5573 (1999).
- ¹⁶ C. M. Hurd, *The Hall Effect in Metals and Alloys* (Plenum Press, New York, 1972).
- ¹⁷ J. Smit, Physica **24**, 39 (1958).

¹⁸ L. Berger, Phys. Rev. B **2**, 4559 (1970).

¹⁹ C. M. Varma, Phys. Rev. B **54**, 7328 (1996).

²⁰ D. Emin, M. Hillery, and N-L. H. Liu, Phys. Rev. B **35**, 641 (1987).

²¹ I. F. Lyuksytov and V. Pokrovsky, Mod. Phys. Lett. B **13**, 379 (1999).

FIGURES

FIG. 1. Hall resistivity ρ_{xy} of a $\text{La}_{0.7}\text{Ca}_{0.3}\text{MnO}_3$ single crystal as a function of field at indicated temperatures (main panel), and the temperature dependence of longitudinal resistivity ρ_{xx} at 0 T and 7 T (inset).

FIG. 2. The activated behavior of Hall coefficient R_H (main panel) and Hall mobility μ_H (inset) above T_C . Above 300 K, the slopes are in accord with small-polaron hopping theory. Also shown in the main panel is the effective activation energy of the conductivity, E_σ^* .

FIG. 3. The anomalous Hall coefficient R_S (symbols) are compared with ρ_{xx} (solid line) and ρ_{xx}^2 (dotted line). The main panel is in a logarithmic scale and the inset is a linear scale plot.

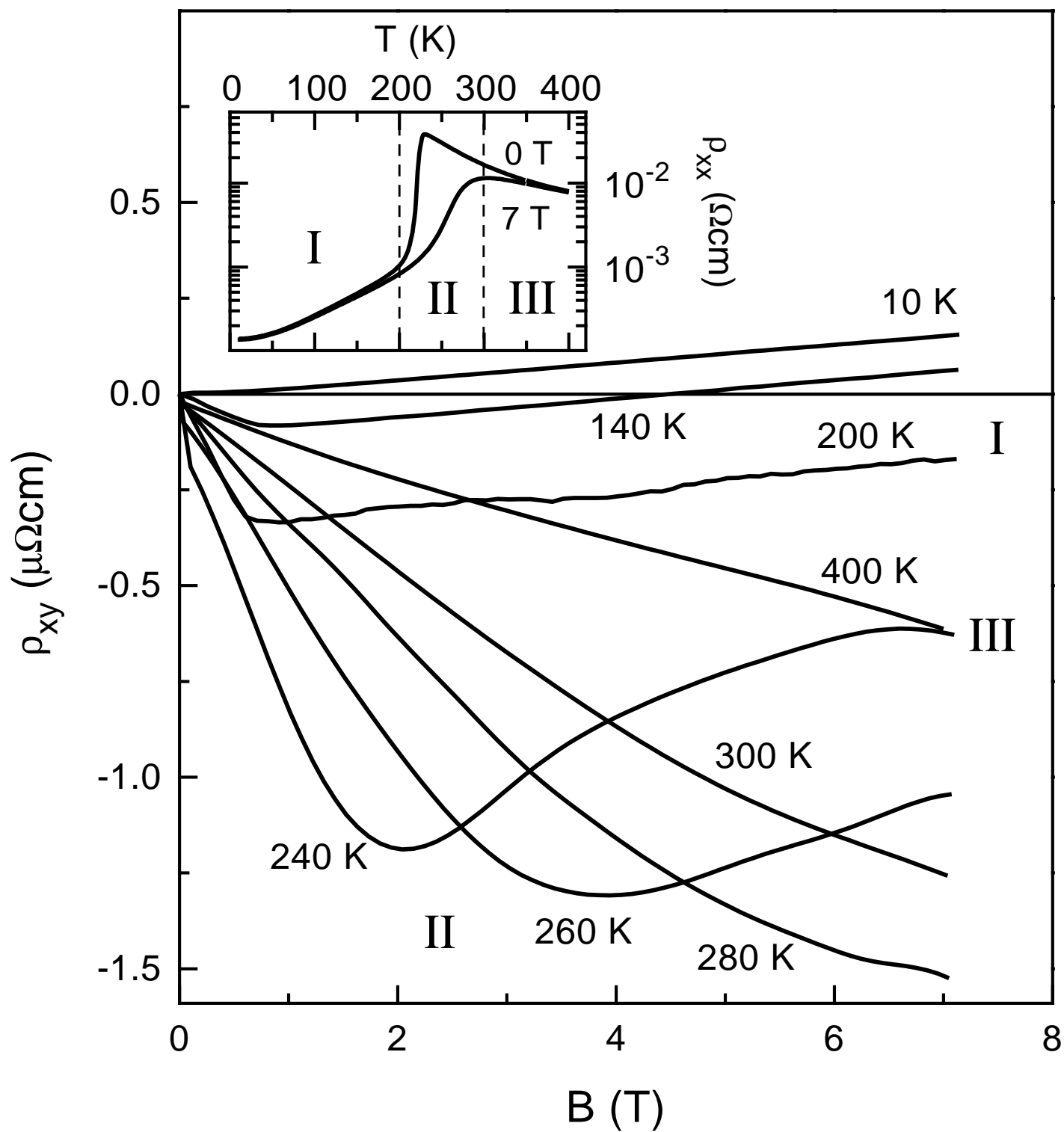


Figure 1, Chun *et al.*

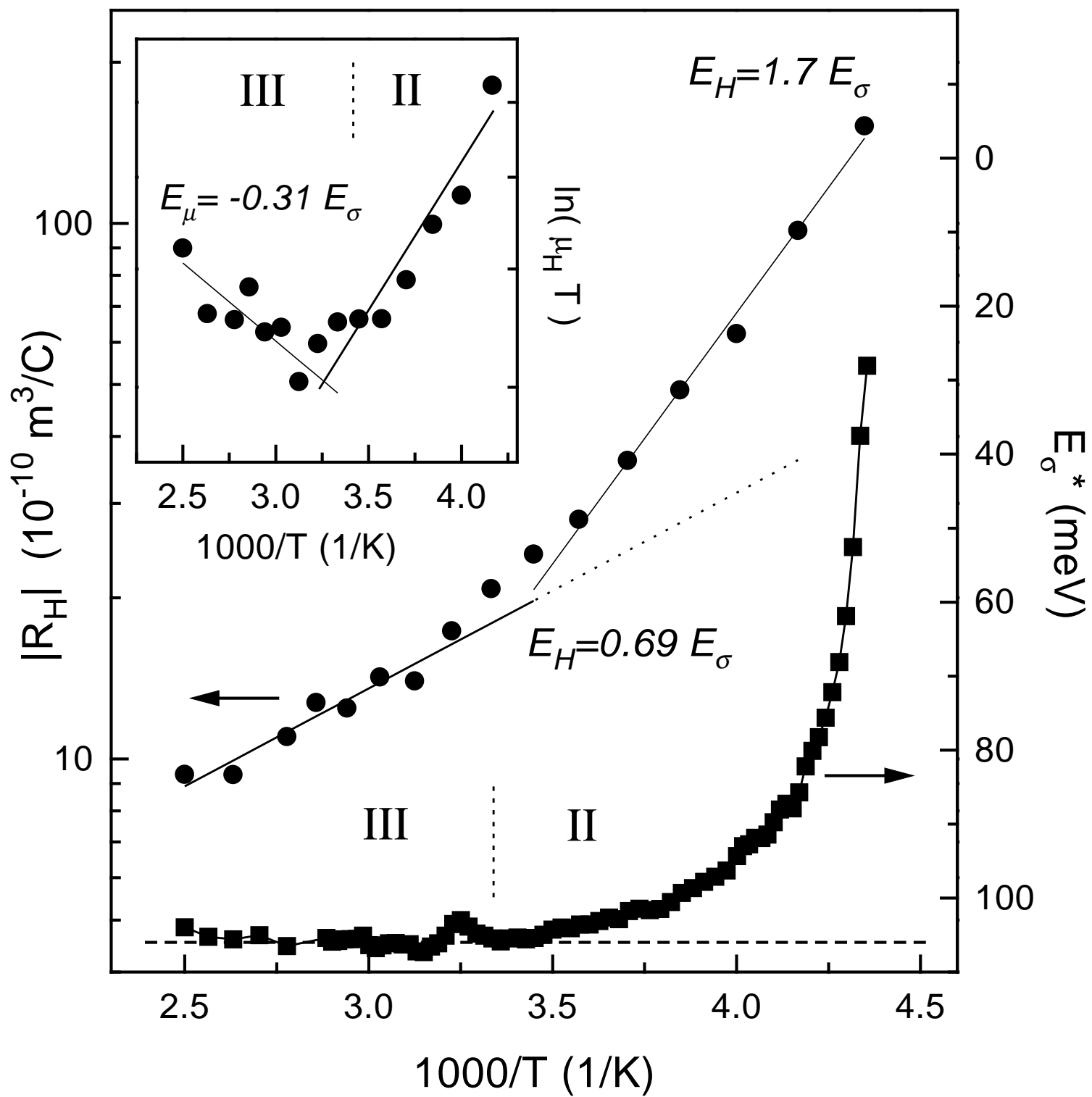


Figure 2, Chun *et al.*

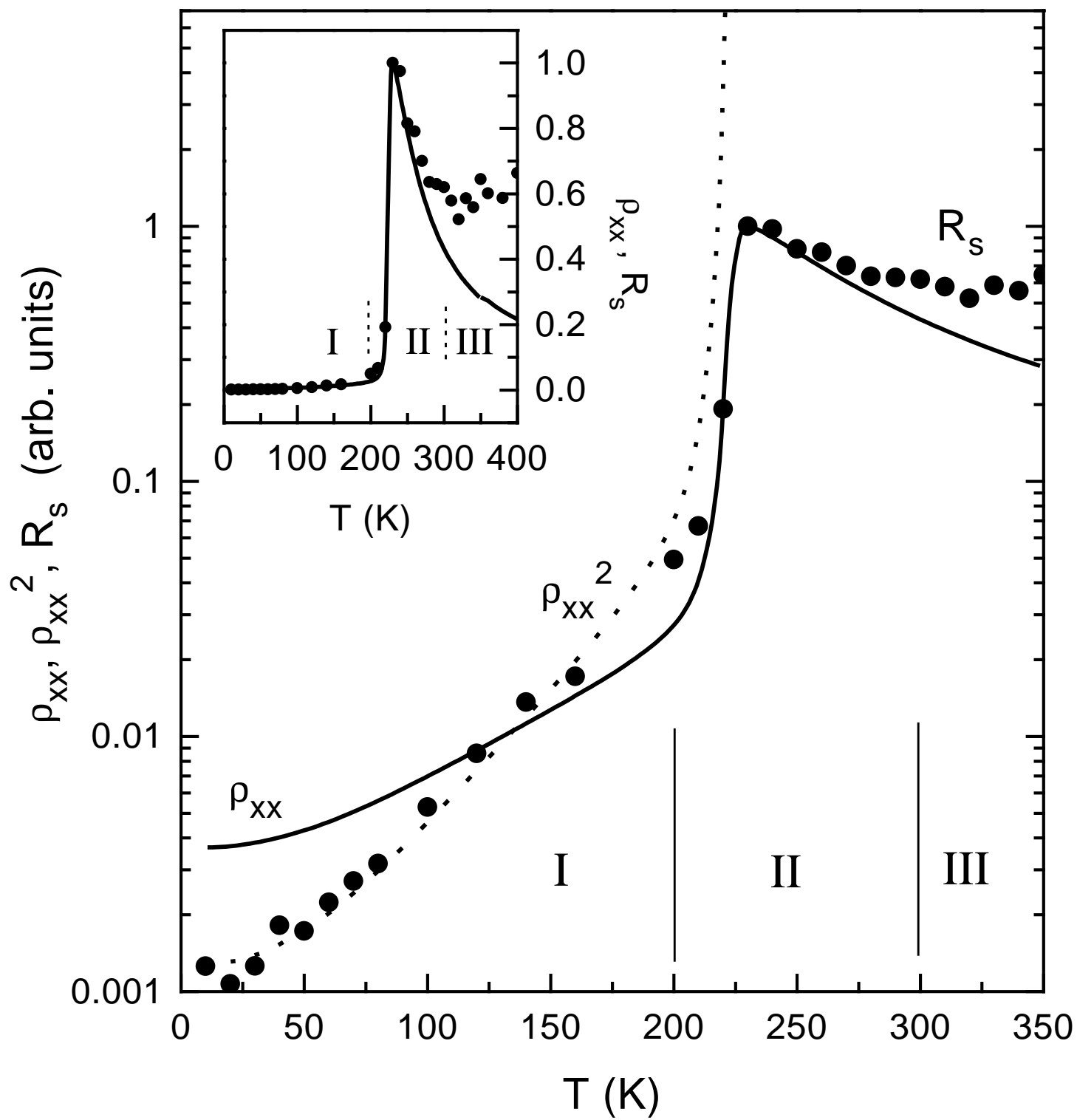


Figure 3, Chun *et al.*